

Digital versus Analog Control of Bilateral Teleoperation Systems: A Task Performance Comparison

Ting Yang^{a, b, *}, Yili Fu^a, Mahdi Tavakoli^{b, *}

^a State Key Laboratory of Robotics and Systems, Harbin Institute of Technology, Harbin, Heilongjiang, 150080, China.

^b Department of Electrical and Computer Engineering, University of Alberta, Edmonton, AB T6G 2V4, Canada.

Email: tyang1@ualberta.ca, ylfms@hit.edu.cn, tavakoli@ece.ualberta.ca

Abstract

Controller discretization has the potential to jeopardize the stability of a bilateral teleoperation system. As reported in the literature, stability conditions impose bounds on the gains of the discrete-time controller and the sampling period and also a trade-off between the two. This paper shows a choice of task for which large sampling periods, necessitating low control gains for maintaining stability, lead to low teleoperation transparency and unacceptable task performance. It continues to show that users can successfully perform the same task if the controller is implemented using analog components. This highlights the advantages of analog haptics in tasks involving the display of highly stiff environments. The paper also highlights the constraints in designing analog haptic teleoperation controllers and proposes design guidelines to address them.

Keywords

Bilateral Teleoperation System; Continuous-time Control; Discrete-time Control; Transparency; Task Performance

1. Introduction

Digital techniques have liberated control designers from time-consuming analog design. However, this means the advantages of analog control have been abandoned [1-4], which may cause significant performance and stability consequences. This paper studies whether an analog controller can achieve better user task performance compared to a digital controller in bilateral teleoperation.

A bilateral teleoperation system consists of three parts shown in Fig. 1: A human operator performing a task on an environment through a teleoperator. The teleoperator itself has three parts: A master user interface for the human operator, a slave robot acting at the environment, and a controller to ensure stability and performance (transparency). The relatively independent workspaces of the master and the slave let bilateral teleoperation be used in harsh, unsafe, remote or confined areas not appropriate for human presence, such as is the case in underwater or space exploration and telesurgery [5].

*Corresponding Author

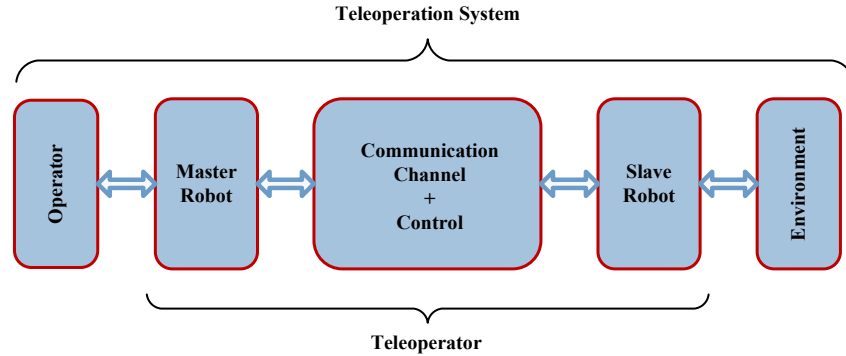


Fig. 1. A teleoperation system block diagram

Controllers in teleoperation systems must satisfy two important indicators, that is, stability and transparency. When we discuss the stability, sometimes passivity of the teleoperator is studied instead [6-10]. Or, the less conservative approach of absolute stability can be utilized [11-15]. Regardless, both approaches indicate that for a stable sampled-data teleoperation system, there needs to be an upper bound on the product of the control gain and the sampling period.

While the stability is a requisite for operation of the system, transparency is the ability of the system to transmit forces and positions from one end to the other end of the system without distortion. It is important to make sure the controller in a teleoperation system is designed such that high transparency is achieved. This will ensure that the human operator can perform a task through a teleoperation system with the same ease and performance that he/she does it in a direct-touch situation. In other words, transparency (system performance) and user task performance go hand in hand.

As will be discussed in Section 3, a larger control gain generally leads to higher system transparency, and therefore, improves user task performance. However, when the teleoperation controller is implemented in discrete-time (D-T), the product of control gain and sampling period is upper bounded as a condition for keeping the system stable. In practice, the value of the sampling period is lower bounded because of the time required for A/D and D/A conversion and the control law implementation, thus resulting in an upper bound on the control gain as far as stability is concerned. A major difficulty arises if this stability-imposed upper bound on the control gain constrains the teleoperation transparency to the level that tasks cannot be completed successfully by the human operator.

One way of solving the aforementioned dilemma is to use fast-sampling processors that provide very small sampling periods [16-19], but this option will be more expensive than the ubiquitous personal computers. Recently, a method is proposed by Susa and Takehana [20], which divides the force presented to the human operator into two parts: a penalty force to render shapes and a vibration force. The penalty forces are unique for different materials, which can be detected from preliminary experiments.

A more affordable way is to use analog components to implement the teleoperation controller. As the analog system does not sample data, it is expected to fundamentally eliminate the limitation brought by the sampling period. This article discusses whether a bilateral teleoperation system with a continuous-time (C-T) analog controller can accomplish tasks requiring high positioning precision (high transparency), which require high-gain control, while maintaining the system stability.

The paper is organized as follows. The bilateral teleoperation system used in this paper is modelled in Section 2. A detailed discussion of stability and transparency conditions needed in our teleoperation system is presented in Section 3. The experimental teleoperation system and the design differences between continuous-time and discrete-time controllers are shown in Section 4. Section 5 presents constraints brought upon by the two classes of controllers. Section 6 provides the control design procedure considering the constraints mentioned above. An empirical approach for designing the continuous-time teleoperation controller is presented in Section 7. Then, the experimental results concerning the teleoperation system performance are shown in Section 8. Further, the parameters of hybrid matrix H of discrete-time controlled and continuous-time controlled teleoperation systems have been found and compared in Section 9. In Section 10, the human performance of a switch-flipping task under continuous-time controlled and discrete-time controlled teleoperation systems is studied and compared. Lastly, concluding remarks are given in Section 11.

The contribution of this paper is in showing that a continuous-time controller can significantly increase the teleoperation system transparency when compared to its discrete-time counterpart (i.e., the discretized version of the same controller). This improvement in teleoperation system transparency is shown via a user study to translate to enhanced user task performance for the particular task considered in the paper. In this way, the paper shows that the root cause of task failure in teleoperation can actually be control sampling (while the blame is routinely placed on ubiquitous non-idealities such as friction, noise, control signal saturation, unmodelled dynamics, communication channel delay, etc. but not on sampling). The continuous-time controller provides these benefits without endangering the system stability. Another contribution of the paper is in providing a systematic design approach for the continuous-time haptic teleoperation controller.

2. System Modeling

In this section, the bilateral teleoperation system used in the subsequent sections is modeled, including the forms of teleoperator, continuous-time dynamics of input-output and discrete-time input-output relations.

2.1 System Modeling

The block diagram of a position-error-based (PEB) bilateral teleoperation system is shown in Fig. 2. Here, F_h is the interaction force between the master robot and the human operator, and F_e is the interaction force between the slave robot and the environment. Also, \tilde{F}_h and \tilde{F}_e represent the exogenous human operator and environment forces, respectively. X_m and X_s denote the position of the master and slave robots, respectively. Z_h and Z_e are the operator and environment impedances, respectively. The continuous-time models of the human operator and the environment are:

$$\begin{aligned}\tilde{F}_h - F_h &= Z_h(s) s X_m \\ \tilde{F}_e - F_e &= Z_e(s) s X_s\end{aligned}\tag{2.1}$$

where s is the Laplace operator.

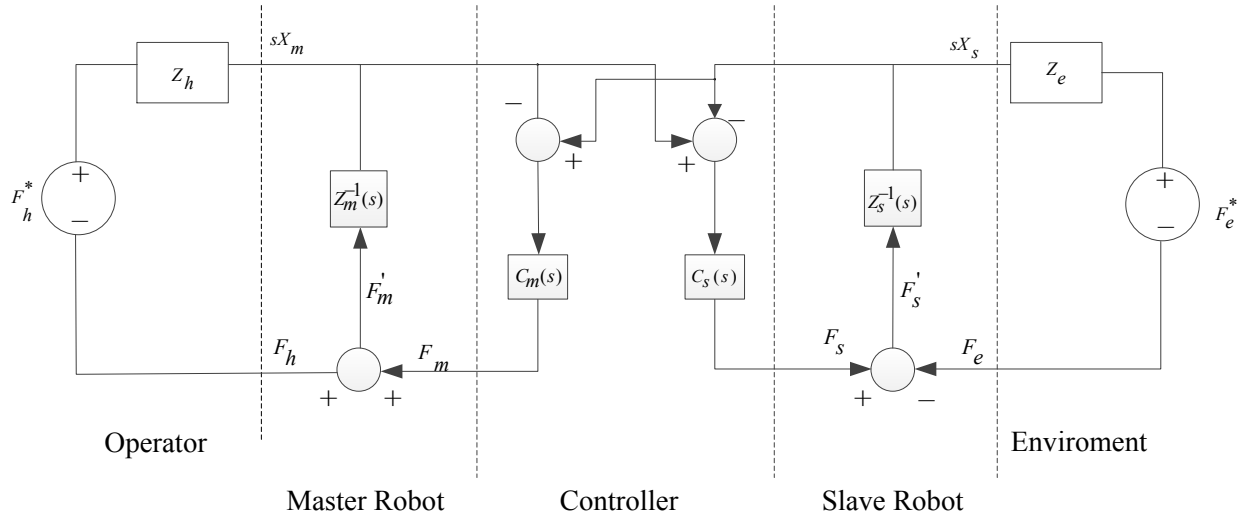


Fig. 2. A PEB bilateral teleoperation system

The continuous-time dynamics of the master and slave robots in the s -domain are:

$$\begin{aligned} sX_m &= Z_m(-F_m + F_h) \\ sX_s &= Z_s(-F_s + F_e) \end{aligned} \quad (2.2)$$

where F_m and F_s are the control signals for the master and the slave, respectively. Z_m , Z_s represent impedances of the master and slave robots and are considered to be:

$$\begin{aligned} Z_m &= \frac{1}{m_m s + b_m} \\ Z_s &= \frac{1}{m_s s + b_s} \end{aligned} \quad (2.3)$$

where m_m and m_s denote the masses of the master and slave robots, and b_m and b_s denote the corresponding damping terms.

The PEB-controlled teleoperator in Fig. 2 can be modelled in the hybrid matrix form:

$$\begin{bmatrix} F_h(s) \\ -sX_s(s) \end{bmatrix} = H(s) \begin{bmatrix} sX_m(s) \\ F_e(s) \end{bmatrix} \quad (2.4)$$

with the following hybrid matrix:

$$H(s) = \begin{bmatrix} h_{11} & h_{12} \\ h_{21} & h_{22} \end{bmatrix} = \begin{bmatrix} Z_m + C_m \frac{Z_s}{Z_s + C_s} & \frac{C_m}{Z_s + C_s} \\ -\frac{C_s}{Z_s + C_s} & \frac{1}{Z_s + C_s} \end{bmatrix} \quad (2.5)$$

In the above, the proportional-derivative (PD) controllers $C_m = (k_{v_m} s + k_{p_m})/s$ and $C_s = (k_{v_s} s + k_{p_s})/s$ are usually used for the master robot and the slave robot, respectively. When implementing these controllers in discrete-time, the sampled-data outputs of the master and slave controllers are [21]:

$$\begin{aligned}
F_m^*(s) &= C_m(z)[X_s^*(s) - n_p X_m^*(s)] \\
F_s^*(s) &= C_s(z)[n_p X_m^*(s) - X_s^*(s)]
\end{aligned}
\tag{2.6}$$

where * shows sampled signals, and n_p defines the position ratio between the master and slave robots.

In this paper, the PEB teleoperation control method is chosen because for direct force reflection (DFR) control, even a continuous-time teleoperation system will not be absolutely stable [15]. Since the study of the stability-transparency tradeoffs caused by sampling and how they limit task performance is of interest, it is appropriate to start with a known and stable continuous-time teleoperation control architecture, namely the PEB control method.

3. Discussion of Stability and Transparency

Details of the stability conditions and transparency of the aforementioned PEB-controlled teleoperation system are shown next.

3.1 Transparency of PEB teleoperation system

In order to obtain satisfactory system transparency and good user performance, perfect correspondence between the master and slave positions and the master and slave forces is required. This amounts to $H(s)$ being as close to

$$H_{ideal} = \begin{bmatrix} 0 & 1 \\ -1 & 0 \end{bmatrix} \tag{3.1}$$

as possible. Evidently, this would happen if the gains in the controllers C_m and C_s are large enough in (2.5). However, as will be shown next, this will pose a problem for stability.

3.2 Stability of PEB teleoperation system

Having modeled a teleoperation system as a two-port network (teleoperator comprising the master, the controller and communication channel, and the slave) coupled to two one-port networks (environment and operator) paves the way for ensuring closed-loop stability via teleoperator absolute stability. The absolute stability of a teleoperator is equal to the stability of the overall teleoperation system assuming that the two one-port terminations are passive but otherwise arbitrary.

3.2.1 Stability of continuous-time PEB teleoperation system

A continuous-time absolute stability criterion was proposed by Llewellyn for two-port networks [22, 23], which can be applied to give closed-form conditions involving the teleoperator's immittance (impedance, admittance, hybrid, or transmission) matrix. For the continuous-time PEB teleoperation system shown in Fig. 2, the teleoperator absolute stability conditions are given below. The PEB teleoperation system of Fig. 2 is absolutely stable if $k_{pm}, k_{vm}, k_{ps}, k_{vs} > 0$ and $C_m(s)/C_s(s) = \alpha$, where α is a positive constant [24].

3.2.2 Stability of discrete-time PEB teleoperation system

In the sampled-data counterpart of the teleoperation system in Fig. 2, the PD controllers are discretized, e.g., using backward difference method[25], to:

$$C(z) = k_v (z-1)/T + k_p \quad (3.2)$$

where $C_m = C_s = C$, $k_{vm} = k_{vs} = k_v$, and $k_{pm} = k_{ps} = k_p$. Then, a sufficient absolute stability condition can be found for the sampled-data teleoperator[15]:

$$\frac{b_m b_s}{b_s + b_m} > \frac{k_v T}{2} + k_p \quad (3.3)$$

where T represents the sampling period. For a given teleoperation system, the left side of (3.3) is fixed. Thus, the stability condition shows the upper bound for $k_v T$.

3.3 Analysis of stability and transparency conditions

Based on the above results for the stability and transparency of a PEB teleoperation system, the discrete-time absolute stability condition (3.3) imposes a trade-off between the sampling period and the proportional gain of PD controllers. This combined with the transparency requirements (i.e., high gains in the PD controllers to make (2.5) approach (3.1)) show a trade-off between stability and transparency for a fixed sampling period. While a larger control gain leads to higher transparency, it can jeopardize the stability of the sampled-data teleoperation system. This is in contrast to the continuous-time control case where there is no constraint put on the controller gains by the stability condition in Theorem 1, and thus no significant stability-imposed constraint on transparency. These show the significance of comparing the system transparency and the task performance achievable with continuous-time versus discrete-time control.

4. Controllers in a Teleoperation System

This section presents our experimental setup and the differences between the two cases of discrete-time and continuous-time control in terms of control design issues. In both cases, the teleoperation system consists of two identical Servo SRV-02 Quick Connect Modules (Quanser Inc., Markham, ON, Canada) as 1-degree-of freedom revolute-joint master and slave robots (Fig. 3). Each of the master and slave modules, which is comprised of a DC motor, a gear, and a potentiometer, is preceded by an *inner* current control loop so that an *outer* position control loop can send torque commands (i.e., F_m and F_s in Fig. 2) to each robot. While the current control loop is always implemented by analog components, the position controller can be implemented either in the continuous-time or the discrete-time domain.

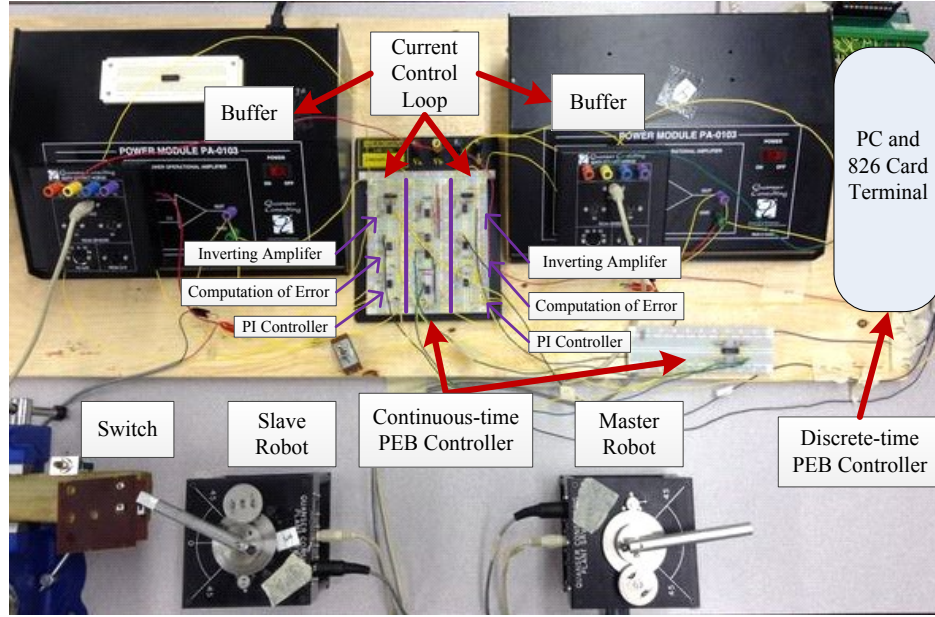


Fig. 3. The experimental setup of bilateral teleoperation system

4.1 Current control loop

The circuit diagram of this current control loop for each motor is shown in Fig. 4. The input voltage V_{ref} is proportional to and represents the set-point value for the current I_M passing through the motor M . More exactly, if the current tracking error is zero, $V_{ref} = (R_{14}R_{13}/R_{12})I_M$ can be found. The voltage V_{ref} is fed to the current control circuit (inner control loop) in Fig. 4 from the circuit in Fig. 5 for the position control loop (outer control loop), which will be discussed later.

In Fig. 4's INVERTING AMPLIFIER block, a voltage proportional to the negative of the actual motor current is generated: $V_{IA} = -(R_{14}R_{13}/R_{12})I_M$. In the COMPUTATION OF ERROR block, V_{ref} representing the desired motor current is compared to V_{IA} representing the actual motor current. If $R_7 = R_8$, then the error voltage $V_E = -(V_{ref} + V_{IA})$ is fed to the PI CONTROLLER block. The proper choice of R_9 , R_{10} , R_{11} and C in the PI CONTROLLER block will ensure a good rise time in current tracking and a tracking error that approaches zero asymptotically. The controller output V_{PI} is then fed to the BUFFER block so that enough current can be supplied to the motor M . Overall, the loop in Fig. 4 will ensure fast and accurate current control for each of the master and slave robots. Because we know the static relationship between the current and torque for the DC motors, each of the robots can now be torque controlled. Section 5 will discuss the constraints and an empirical approach for the design of this current control loop.

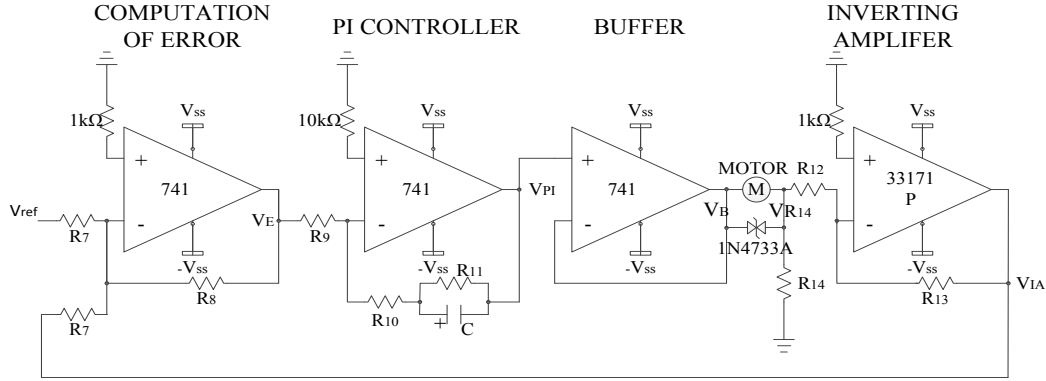


Fig. 4. Circuit diagram of Current Control Loop

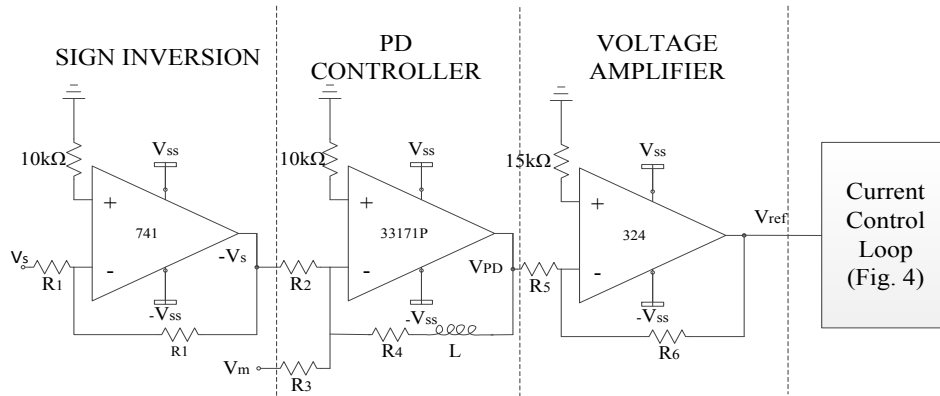


Fig 5. Circuit diagram of a continuous-time position controller C_s

4.2 Position control loop

Having ensured in Section 4.1 that the master and slave robots are torque controlled, now the PEB teleoperation control system in Fig. 2 needs to be implemented. Whether the position controllers $C_m(s)$ and $C_s(s)$ embedded in this PEB system are implemented in discrete-time or in continuous-time will lead to two cases. The main difference between discrete-time and continuous-time control is the use of analog components in making the latter.

4.2.1 Discrete-time position control

Digital signals are processed in a PC with a dual-core AMD Opteron Processor 270 at 1.99GHz with a 64-bit Windows 7 operating system. A Model 826 multifunction analog/digital I/O card (Sensoray Co., Tigard, OR, USA) is used for A/D and D/A conversion. Master and slave positions are acquired following A/D conversion of potentiometer voltages. The position error is then fed to the discrete-time PD controller (2.6) for each of the master and slave robots. Following D/A conversion, the control signals F_m and F_s are output to the master and slave robots, respectively. The sampling frequency is 1000 Hz.

4.2.2 Continuous-time position control

The PD controller $C_s(s)$ in Fig. 2 will now be realized using the circuit shown in Fig. 5, and a similar circuit will be used for implementing $C_m(s)$. In Fig. 5, V_s represents the voltage

readout from the potentiometer of the slave robot. Following a sign inversion, $-V_s$ is compared to V_m , which denotes the potentiometer voltage read from the master robot. Therefore, $V_m - V_s$ is input to the PD Controller block (R_2 and R_3 can be chosen differently if position scaling between the master and slave robots is desired). When $R_2 = R_3$, the controller's transfer function (incorporating the PD Controller and Voltage Amplifier blocks) will be:

$$C_s(s) = \frac{R_6}{R_5} \left(\frac{R_4 + sL}{R_2} \right) \quad (4.1)$$

5. Constraints in the Design of Controllers in a Teleoperation System

Finding appropriate values of resistors and an inductance to generate the required control gains needs due attention in the case of analog control implementation. For instance, it is important to avoid saturating the operational amplifier or over-loading the motors while achieving accurate (high-gain) current and position control. In the following, such design constraints will be discussed in detail.

5.1 Constraints in the current control loop design

There are several constraints when designing the current control loop in Fig. 4. A list of these constraints and how they guide the control design are listed below.

- **Op-amp Saturation Protection:** Saturating the outputs of the op-amps should be avoided in order to maintain their linear operation. This means that the op-amp outputs must always be kept less than or equal to the supply voltage. The following three conditions are needed to avoid the saturation of the four op-amps in Fig. 4 (from left to right, respectively, with the middle two op-amps grouped together):

$$|V_E| = \left| \frac{R_8}{R_7} (V_{ref} + V_{LA}) \right| \leq V_{ss} \quad (5.1)$$

$$|V_{PI}| = |V_B| = \left| \left(\frac{R_{10}}{R_9} + \frac{1/(R_9 C)}{(1/(R_{11} C)) + s} \right) V_E \right| \leq V_{ss} \quad (5.2)$$

$$|V_{LA}| = \left| V_{R_{14}} \frac{R_{13}}{R_{12}} \right| \leq V_{ss} \quad (5.3)$$

- **Motor Over-load Protection:** Over-loading the DC motor beyond its rating should be avoided in order to prevent motor burnout. Accordingly, the voltage across the DC motor terminal should be less than or equal to its nominal voltage. Additionally, the current passing through the armature should not exceed the stall current (the current the motor will draw under maximum torque conditions). If the stall current (or torque) information is not provided, either the motor's power rating or the armature resistance value can be used in combination with the nominal voltage value to estimate the nominal current for the motor. Then, according to Fig. 4, the following conditions need to be satisfied:

$$|V_{MOTOR}| = |V_B - V_{R_{14}}| \leq V_{max} \quad (5.4)$$

$$\left| \frac{V_{R_{14}}}{R_{14}} \right| \leq I_{\max} \quad (5.5)$$

where V_{\max} and I_{\max} are the aforementioned maximum terminal voltage and armature current for the DC motor.

5.2 Constraints in the position controller design for a single robot

There are more constraints when designing the circuits in Fig. 5 for position control of a DC motor.

- **Op-amp Saturation Protection:** Similarly, the following three conditions are needed to avoid the saturation of the three op-amps in Fig. 5 (from left to right, respectively):

$$|V_s| \leq V_{ss} \quad (5.6)$$

$$|V_{PD}| = \left| (R_4 + sL) \left(\frac{V_s}{R_2} - \frac{V_m}{R_3} \right) \right| \leq V_{ss} \quad (5.7)$$

$$|V_{ref}| = \left| \frac{R_6}{R_5} V_{PD} \right| \leq V_{ss} \quad (5.8)$$

5.3 Constraints in the haptic teleoperation controller design for two robots

There are additional constraints in terms of designing circuits in Fig. 4 and Fig. 5 that are imposed when using a DC motor as a haptic master device and another DC motor as the slave robot. Typically, the master robot is force (current) controlled while the slave robot is position controlled. Thus, the following considerations apply to Fig. 4 and Fig. 5, respectively.

- **Large Force Reflection by the Master:** For the DC motor acting as the master, a specific maximum producible torque should be ensured. This will ensure the ability to recreate the feeling of hard-contact tasks for the human operator manipulating the master. Knowing the motor torque constant K and the gear ratio K_g , this results in a specific peak being required for the motor current. This means that, in Fig. 4, V_{ref} will need to go as high as a certain value (determined by $V_{ref} = (R_{14}R_{13}/R_{12})I_M$) without violating the constraints listed in Section 5.1 for op-amp saturation protection and motor over-load protection. If this peak torque is insufficient for doing a certain task, the gear ratio must be increased.

- **Accurate Position Control of the Slave:** For the DC motor acting as the slave, the position control in Fig. 5 has a gain from the input $V_m - V_s$ to the output V_{ref} that may need to be bigger than a certain value for the task to be feasible (e.g., for tasks involving precise positioning and, therefore, high control gains). Again taking $R_2 = R_3$, this gain can be calculated as

$$\frac{|V_m - V_s|}{|V_{ref}|} = \frac{R_5}{R_6} \cdot \frac{1}{R_4 + sL} \quad (5.9)$$

6. Design Procedure for Controllers in a Teleoperation System

In this section, the above constraints will be applied to our experimental setup in Fig. 3 and we will provide design guidelines to satisfy them. The complete design flow chart is presented in Fig. 6. The corresponding give detailed explanations for the *inner* current control loop and the *outer* position controller in 6.1 and 6.2 respectively.

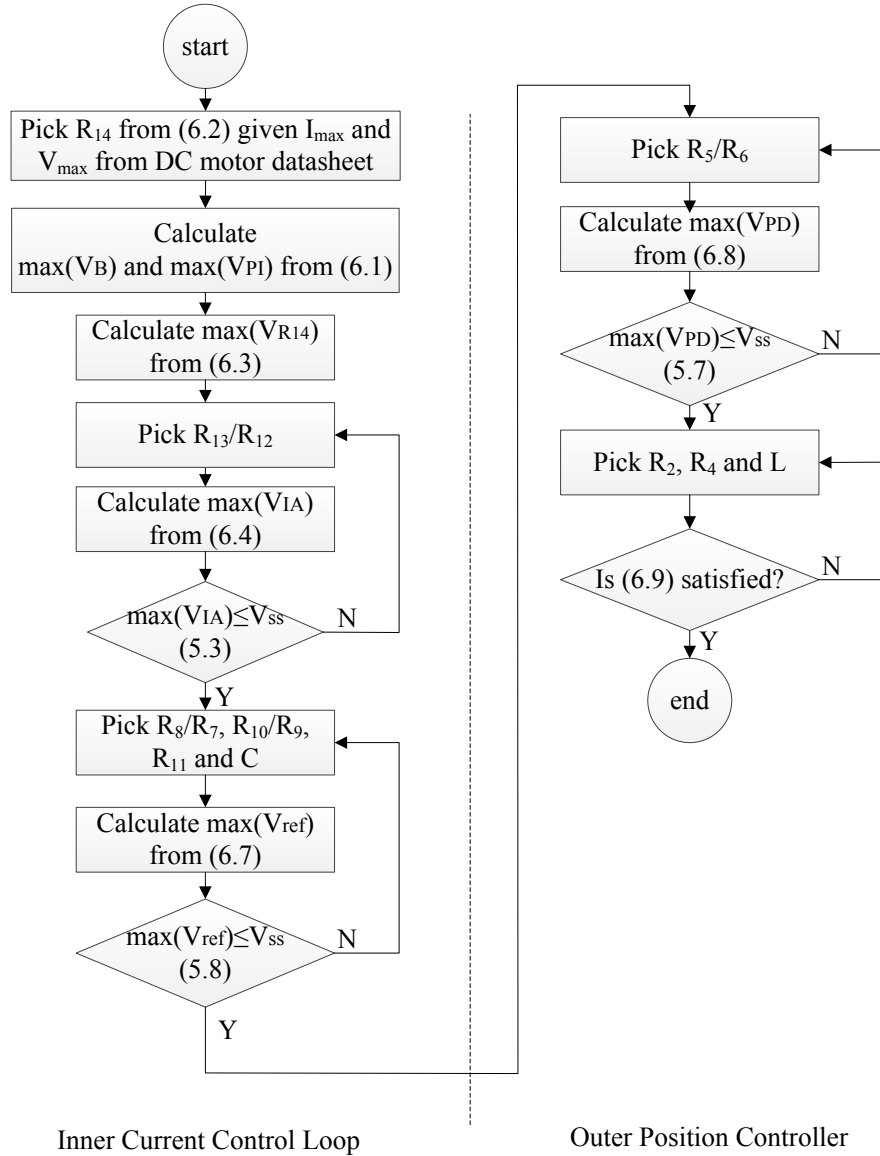


Fig. 6 Flow chart for design procedure

6.1 Design procedure of the current control loop

In Fig. 4, the bias voltage is V_{ss} and the nominal voltage for the DC motor in the Servo SRV-02 module is V_{\max} , which is given in the DC motor datasheet. With the armature resistance R_M , the maximum current to pass through the armature is $I_{\max} = V_{\max}/R_M$. The motor current is the same as the current passing through R_{14} .

According to (5.5), to avoid op-amp saturation under the peak motor current, the current control loop needs to satisfy

$$\max(V_{PI}) = \max(V_B) = V_{\max} + R_{14} \cdot I_{\max} \leq V_{ss} \quad (6.1)$$

Thus, the first step of designing the current control loop is to define the value of R_{14}

$$R_{14} \leq \frac{V_{ss} - V_{\max}}{I_{\max}} \quad (6.2)$$

Once the value of R_{14} is chosen, the maximum value of V_B and V_{PI} can be calculated from (6.1).

With the value of R_{14} , $\max(V_{R_{14}})$ can be calculated from (5.5) as

$$\max(V_{R_{14}}) = R_{14} I_{\max} \quad (6.3)$$

Taking into account (6.3), the following equation can be found from (5.3):

$$\max(V_{IA}) = R_{14} I_{\max} \times \frac{R_{13}}{R_{12}} \quad (6.4)$$

If $\max(V_{IA}) \leq V_{ss}$, the ratio of $\frac{R_{13}}{R_{12}}$ is appropriate, otherwise they need to be reselected such that this inequality condition is satisfied.

Substituting V_E from (5.1) in (5.2) and combining the result with (6.1), the following condition is obtained:

$$\left| V_{ref} + V_{IA} \right| \cdot \left| \frac{R_8}{R_7} \left(\frac{R_{10}}{R_9} + \frac{1/(R_9 C)}{(1/(R_{11} C)) + s} \right) \right| \leq \max(V_{PI}) \leq V_{ss} \quad (6.5)$$

V_{ref} and $V_{R_{14}}$ (or the current passing through the motor) are going to be of the same sign, which means that V_{ref} and V_{IA} will have opposite signs. Thus, $|V_{ref} + V_{IA}| = \left| |V_{ref}| - |V_{IA}| \right|$. By $\left| |V_{ref}| - |V_{IA}| \right| \geq |V_{ref}| - |V_{IA}|$, (6.5) can be turned into

$$\left(|V_{ref}| - |V_{IA}| \right) \left| \frac{R_8}{R_7} \left(\frac{R_{10}}{R_9} + \frac{1/(R_9 C)}{(1/(R_{11} C)) + s} \right) \right| \leq \max(V_{PI}) \quad (6.6)$$

With the maximum **values** of V_{PI} and V_{IA} , the maximum value of V_{ref} can be determined by (6.6) as

$$\max(V_{ref}) = \frac{\max(V_{PI})}{\left| \frac{R_8}{R_7} \left(\frac{R_{10}}{R_9} + \frac{1/(R_9 C)}{(1/(R_{11} C)) + s} \right) \right|} + \max(V_{IA}) \quad (6.7)$$

If $\max(V_{ref}) \leq V_{ss}$, the ratio of $\frac{1}{\left| \frac{R_8}{R_7} \left(\frac{R_{10}}{R_9} + \frac{1/(R_9 C)}{(1/(R_{11} C)) + s} \right) \right|}$ picked in (6.7) is appropriate,

otherwise the ratio of $\frac{R_8}{R_7}$, $\frac{R_{10}}{R_9}$, R_{11} and C need to be chosen once again to satisfy the inequality condition.

This concludes the design of inner current control loop components in Fig. 4.

6.2 Design procedure for the continuous-time position controller

In Fig. 5, the bias voltage is also V_{ss} . According to (5.8) and (6.7), $|V_{ref}| = \left| \frac{R_6}{R_5} V_{PD} \right| \leq \max(V_{ref}) \leq V_{ss}$ needs to be satisfied. Combining with (5.7), the following relationship can be found

$$|V_{PD}| = \left| (R_4 + sL) \left(\frac{V_m}{R_3} - \frac{V_s}{R_2} \right) \right| \leq \frac{R_5}{R_6} \times \max(V_{ref}) \quad (6.8)$$

If $\max(V_{PD}) \leq V_{ss}$, the ratio of $\frac{R_5}{R_6}$ picked is appropriate in (6.8), otherwise they need to be reselected until the inequality condition is satisfied.

For the special case of $R_2 = R_3$, the following condition can be obtained:

$$|V_m - V_s| \leq \frac{R_2 \times \max(V_{PD})}{R_4 + sL} \quad (6.9)$$

By picking the proper ratio of $\frac{R_2}{R_4 + sL}$ in (6.9), it can be ensured that the difference in the initial positions of the master and slave robot (or transient position errors) do not cause op-amp saturation.

7. Case Study: Design of Continuous-time Current and Position Controllers

This section shows the empirical choices of analog components regarding the design procedure mentioned above. First of all, the motor voltage protection needs to be considered. The nominal voltage for the DC motor is $V_{max} = 6V$. If the voltage on the motor is higher than $6V$, the motor will be burnt. In case of this situation, two zener diodes have been added between the motor terminals for voltage protection. Two cascaded zener diodes 1N4733A with opposite polarities break at $5.1V + 0.7V = 5.8V$. Next, we start with the empirical design of the inner current control loop in Fig. 4. Then, we will proceed to the design of the outer position controller in Fig. 5.

7.1 Parameter choices in the current control loop

Now, let us choose the circuit components such that the above conditions are met. In Fig. 4, $V_{ss} = 12V$. According to the DC motor datasheet, the nominal voltage of the DC motor is $V_{max} = 6V$ and the armature resistance is $R_M = 2.6\Omega$, thus the armature's maximum current is $I_{max} = 6V / 2.6\Omega = 2.3A$. Based on (6.2), the current passing through R_{14} is the motor current

$$R_{14} \leq \frac{12V - 6V}{2.3A} = 2.6\Omega \quad (7.1)$$

Thus, the value of R_{14} can be no more than 2.6Ω . The resistance R_{14} has been cascaded with the motor armature to sense the motor current, which means it is desirable to keep R_{14} as small as possible in order not to disrupt the operation of the motor. Here, let us choose $R_{14} = 0.3\Omega$.

Combining (6.1) with (7.1), the maximum value of V_{PI} and V_B will be

$$\max(V_{PI}) = \max(V_B) = 6.69V \quad (7.2)$$

According to (6.3), the maximum value of $V_{R_{14}}$ can be

$$\max(V_{R_{14}}) = 0.3\Omega \times I_{\max} = 0.69V \quad (7.3)$$

Let $\frac{R_{13}}{R_{12}} = 10$, (6.4) becomes

$$\max(V_{IA}) = 0.69 \times \frac{R_{13}}{R_{12}} = 6.9V \quad (7.4)$$

which also meets the demands of $\max(V_{IA}) \leq V_{ss}$ in (5.3).

Substituting $\max(V_{PI})$ from (7.2) in (6.7), for any $R_7 = R_8$ and for $R_9 = 47k\Omega$, $R_{10} = 270k\Omega$, $R_{11} = 1k\Omega$ and $C = 1\mu F$, (6.7) simplifies to:

$$\max(V_{ref}) \leq \left(\frac{6.69}{5.7 + \frac{21.3}{1000 + s}} \right) + \max(V_{IA}) \quad (7.5)$$

Also, satisfying $\max(V_{ref}) \leq V_{ss}$ is seen if (7.4) and (7.5) are combined:

$$|V_{ref}| \leq 7.1V \quad (7.6)$$

This concludes the choice of the components in Fig. 4.

7.2 Parameter choices in the position control loop

In Fig. 5, $V_{ss} = 12V$. Combining with (7.6), (6.8) becomes

$$|V_{PD}| = \left| (R_4 + sL) \left(\frac{V_s}{R_2} - \frac{V_m}{R_3} \right) \right| \leq \frac{R_5}{R_6} \times 7.1V \quad (7.7)$$

when $R_2 = R_3$:

$$|V_s - V_m| \leq \frac{R_5}{R_6} \times \frac{R_2}{R_4 + sL} \times 7.1V \quad (7.8)$$

The maximum difference between the master and slave positions (potentiometer voltages) happen when the two robots are at the opposite and extreme ends of their workspaces. Therefore, $|V_m - V_s|$ can be found empirically and then used in (7.8) to properly choose R_2 , R_4 , R_5 , R_6 and L . Note that because of closed-loop control, the actual upper bound on $|V_m - V_s|$ may be much smaller, allowing more relaxed choices for the components in (7.8).

Another consideration is whether the output force can satisfy the task requirements. The gear ratio on the Servo SRV-02 motor is $K_g = 5 \times 14 = 70$. With the motor torque constant of $K = 0.00767 \text{ Nm/A}$, the maximum torque is $T_{\max} = 70 \times 0.00767 \times I_{\max} = 1.2 \text{ Nm}$. With L being the length of the bar attached to each of the master and slave motors' shafts, the maximum output force of the motors will be $F_{\max} = T_{\max} / L = 10 \text{ N}$. This is acceptable because human operators normally perform manipulation tasks with forces in the range of $2 \text{ N} \sim 10 \text{ N}$, which means this teleoperation system can be used to perform tasks normally performed by humans.

8. Experimental Evaluation of System Stability and Transparency

In this section, the maximum stable controller gains are first tested when the human operates the master robot and the slave robot interacts with the environment (Fig. 3). In this section, the slave's environment is free space.

8.1 Stability of discrete-time teleoperation

A series of experiments were conducted to find the maximum stable control gains under different sampling times. The theoretical stability condition (3.3) is shown in Fig. 7. In the experiment, with a fixed controller gain and sampling period, the master robot is manipulated by the human operator while the slave robot is in free motion. If the master's and/or the slave's positions become unbounded or oscillate indefinitely, the teleoperation system is judged to be unstable – at each tested sampling period, the unstable experiment with the minimum control gain is marked by a square in Fig. 7. If the robots' positions remain bounded, the teleoperation system is judged to be stable – at each tested sampling period, the stable experiment with the maximum control gain is marked by a triangle in Fig. 7. As expected, the experimentally-obtained circles and squares lie close to the theoretically-derived stability boundary.

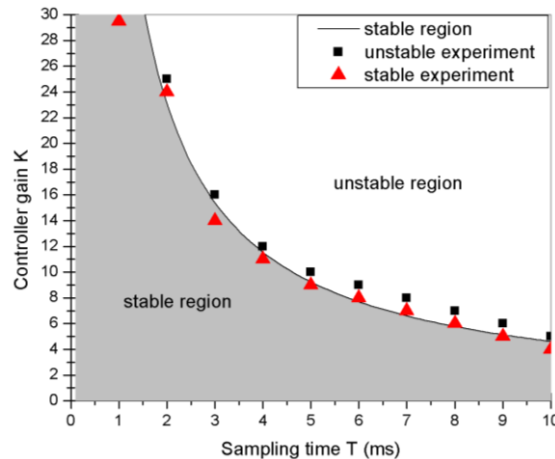


Fig. 7. The theoretical absolute stability region in the K - T plane versus experimental data points obtained from tests on the sampled-data teleoperator.

8.2 Relationship between the control gain and position error

As explained in Section 3.4, larger control gains are expected to increase the transparency of the teleoperation system. This includes lowering the position error between the master and slave robots.

8.2.1 Performance of Discrete-time teleoperation in free motion

For discrete-time teleoperation, with a fixed small sampling period $T = 1ms$, the task performance under various controller gains that satisfy the stability condition (3.3) is tested. Since (3.3) imposes an upper bound of 20 on the control gain for stability reasons, Fig. 8 shows the master-slave position tracking results for control gains of 1, 10 and 20. When $K > 20$ the system is theoretically outside of stable region specified by (3.3), and experimentally the system becomes unstable.

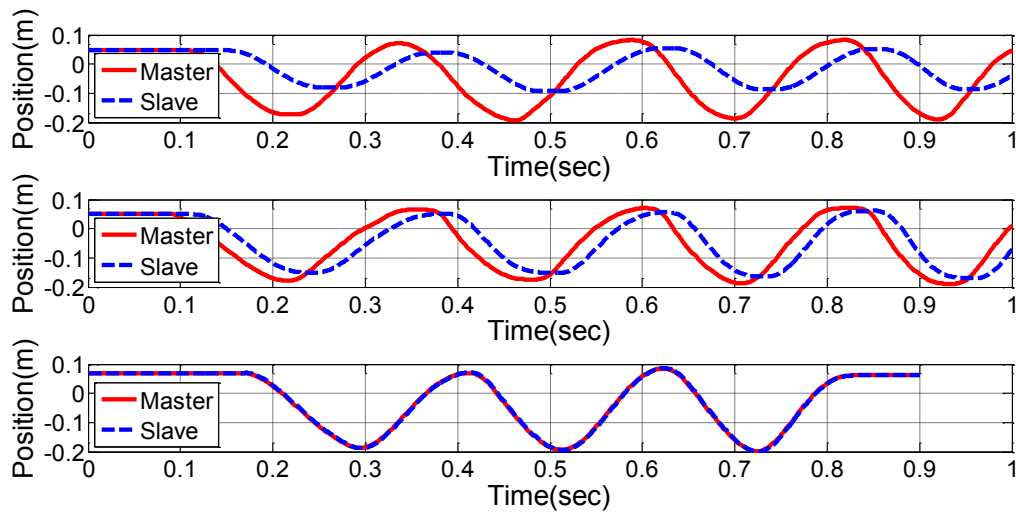


Fig. 8. Master-slave position tracking profiles when the operator moves the master and the slave is in free space in discrete-time teleoperation. The proportional controller gains are $C = 1.0$, $C = 10$, $C = 20$ for (a) - (c), respectively. The corresponding Euclidean norms of the position tracking errors between the master and the slave are 0.7626, 0.5885 and 0.0089.

8.2.2 Performance of Continuous-time teleoperation in free motion

With the teleoperation controller also implemented using analog electronic components, various continuous-time controller gains are also tested in order to show the relationship between the control gain and position error. Fig. 9 shows the master-slave position tracking results for control gains of 10, 100 and 300. While in theory there is no upper bound on the control gain for stability, in practice there is a maximum value for the gain (due to op-amp saturation).

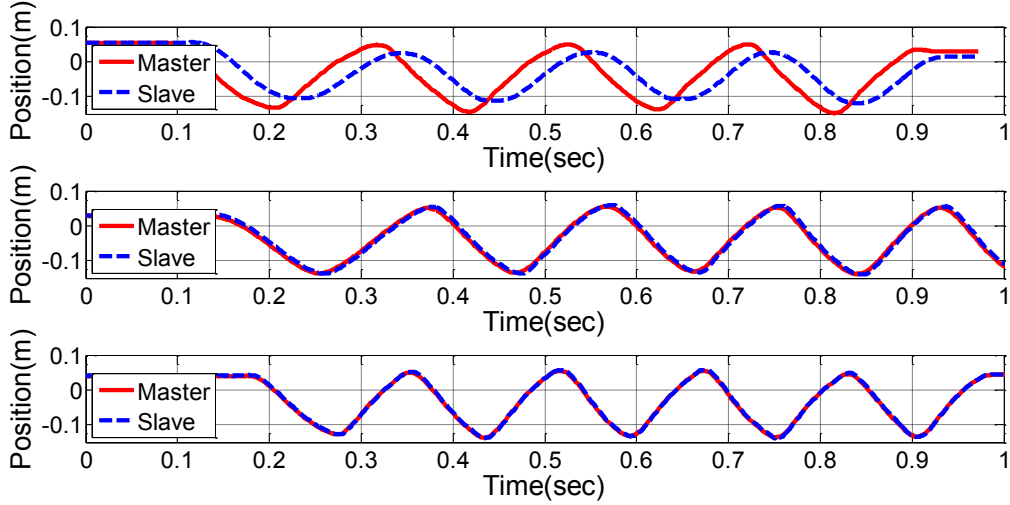


Fig.9. Master-slave position tracking profiles when the operator moves the master and the slave is in free space in continuous-time teleoperation. The proportional controller gains are $C = 10$, $C = 100$, $C = 300$ for (a) - (c), respectively. The corresponding Euclidean norms of the position tracking errors between the master and the slave are 0.7197, 0.0520 and 0.0204.

It can be seen from Fig. 8 and Fig. 9 that in both the continuous-time and discrete-time systems, larger control gains always corresponds to smaller position tracking error. Interestingly, small master-slave position tracking errors are sometimes the key to the successful performance of certain tasks such as the one discussed in the Section 10.

9. Hybrid parameter comparison between discrete-time and continuous-time teleoperation systems

To further evaluate the transparency differences between the discrete-time controlled and the continuous-time controlled teleoperation systems, we use the hybrid representation given by (2.4) and (2.5) to obtain

$$\begin{aligned} F_h &= h_{11} \cdot sX_m + h_{12} \cdot F_e \\ -sX_s &= h_{21} \cdot sX_m + h_{22} \cdot F_e \end{aligned} \quad (9.1)$$

Each element of the H matrix has a physical meaning. The hybrid parameter $h_{11} = F_h/sX_m|_{F_e=0}$ is the input impedance felt by the operator in the free-motion condition. The parameter $h_{12} = F_h/F_e|_{sX_m=0}$ is a measure of force tracking in the haptic teleoperation system when the master is locked in motion. The parameter $h_{21} = -X_s/X_m|_{F_e=0}$ is a measure of the position (velocity) tracking performance when the slave is in free space. The parameter $h_{22} = -sX_s/F_e|_{sX_m=0}$ is the output admittance when the master is locked in motion. Equation (3.1) gives the hybrid parameter values for perfect transparency. Nonzero values for h_{11} mean that even when the slave is in free space, the user will receive some force feedback. Nonzero values for h_{22} mean that when the master is locked in place, the slave will move in reaction to slave/environment contacts. Deviations from 1 and -1 for h_{12} and h_{21} indicate imperfect force tracking and position tracking between the master and slave robots, respectively.

Two different kinds of tests have been performed to find the hybrid parameters. First, in free-motion tests, a human operator moves the master robot back and forth for about 1 minute while the slave robot moves in free space. Since $F_e = 0$, the frequency responses $h_{11} =$

F_h/sX_m and $h_{21} = -X_s/X_m$ can be found by applying spectral analysis (MATLAB function *spa*) on the free-motion test data. Second, other tests are done by fixing the master robot to a wall while trying to move the slave robot by applying forces on it. Since $X_m = 0$, the frequency responses $h_{12} = F_h/F_e$ and $h_{22} = -sX_s/F_e$ can be found. In the above two tests, the force data concerning external interactions of master robot and slave robots are recorded by two JR3 force sensors. The largest control gains for the two teleoperation systems under stable conditions were obtained from Section 8 and used in the two tests; this is a gain of 20 for discrete-time controlled system with 1 millisecond sampling period, and a gain of 300 for the continuous-time controlled system.

The magnitudes of the hybrid parameters of the two teleoperation systems are shown in Fig. 10. As can be seen in Fig. 10, the continuous-time controlled teleoperation system shows its superiority in terms of transparent performance considering the ideal transparency requirement (3.1).

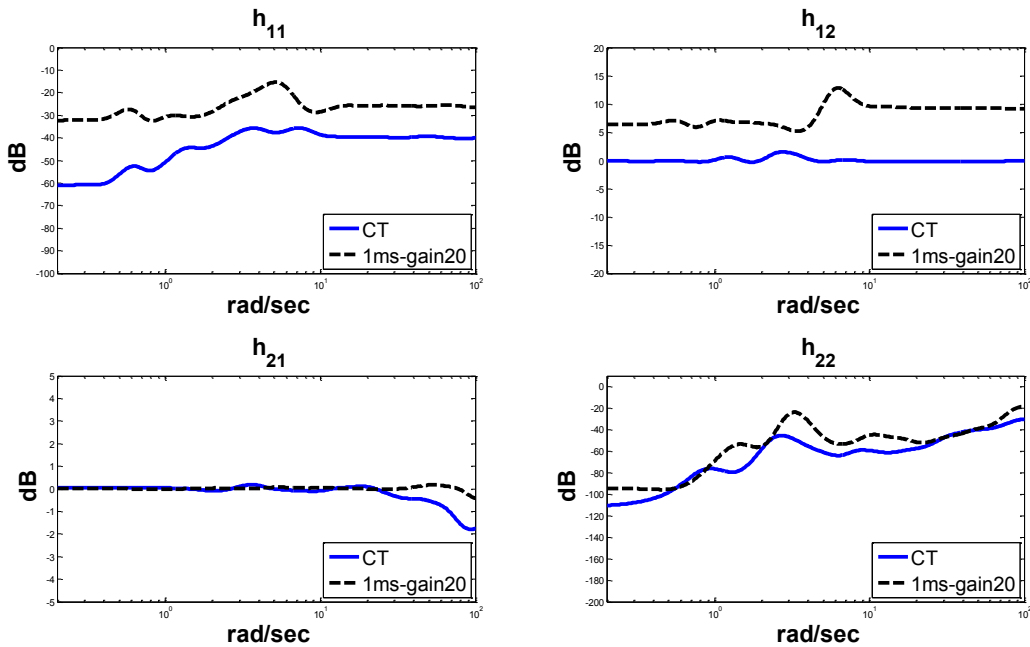


Fig.10. Magnitudes of the hybrid parameters for the teleoperation systems: (solid) continuous-time controlled system, (dashed) discrete-time controlled system.

The relatively high value of h_{11} for the discrete-time controlled system is evidence of the fact that the system gives a “sticky” feel of free-motion movements to the operator; the feeling of the free-motion condition will be more realistic under continuous-time control. The better force tracking performance of the continuous-time teleoperation system, i.e., $h_{12} \approx 0$ dB, demonstrates a better force tracking performance for the continuous-time controlled system. With regard to h_{21} , both spectra are close to 0 dB, indicating both systems can ensure good position tracking in free space; this is in accordance with the result in the Fig. 8 (c) and Fig. 9 (c). With regard to h_{22} , the values are again more or less similar for the two systems. Overall, these results demonstrate that a continuous-time controller can significantly increase the system transparency without sacrificing the stability of the teleoperation system.

10. Human task performance in teleoperated flipping of a switch

To demonstrate the superior performance of a continuous-time controlled teleoperation system compared to the case of discrete-time control, let us consider a stiff task. Consider a teleoperated switch-flipping task, where the user needs to flip the switch in Fig. 11 from position 1 to position 2 but not to position 3. In order to achieve this aim in the teleoperation mode, the master/slave position tracking error, which is influenced by the teleoperation controller performance, should be no more than the distance between positions 2 and 3 of the switch. Evidently, successful user task performance goes hand in hand with high system transparency for this task.

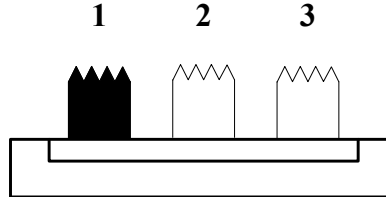


Fig. 11. A three-way switch.

Considering the discussion in Section 3.3, the only way to reach such a small position error is to have a sufficiently large control gain, which may risk instability in the case of discrete-time control. Here, the performance of sampled-data and continuous-time teleoperation are compared to see whether their maximum gain obtained in Section 8.1 could meet the requirements of successful task performance while preserving stability.

In the following, the sampled-data and continuous-time teleoperation are compared in terms of system performance and human task performance. The system performance is measured by the master-slave position tracking error, which as explained above is key to the successful performance of the switch-flipping task. The human task performance is measured by human factors experiments in which the success rate of human subjects in performing the switch-flipping task is measured and compared under sampled-data and continuous-time teleoperation.

10.1 Teleoperation system performance

The system performances under discrete-time and continuous-time controlled bilateral teleoperation are first. In this study, there is a need to eliminate the influence of the human operator for a fair comparison. The configuration in Fig. 12 is used to replace the human operator, where a weight m is connected to the handle of the master robot through a pulley and rope mechanism. Evidently, the “operator” force applied on the master robot is always the same across different experiments. In this way, it is possible to do a fair comparison of system performance between discrete-time versus continuous-time control.

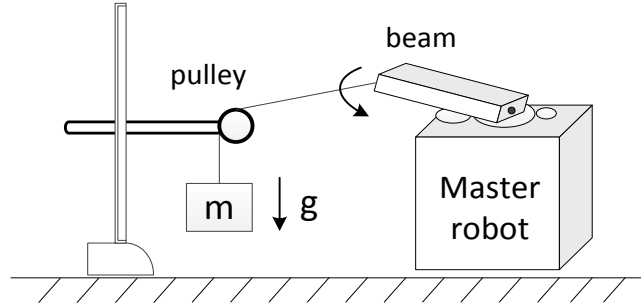


Fig. 12. Achieving repeatable inputs applied to the master robot.

Fig. 13 shows the master-slave position tracking errors of the two systems with their maximum, admissible (i.e., stability-preserving) control gains. It can be seen that for the same input force applied on the master robot, the position tracking errors between the master robot and the slave robot are 0.02 and 0.18 under continuous-time and discrete-time control, respectively. Clearly, freeing up the teleoperation system from the sampling-imposed limitations in terms of the control gain upper bound has a significant effect on the system performance. In the next section, we will investigate if this also translates into actual task performance success rates.

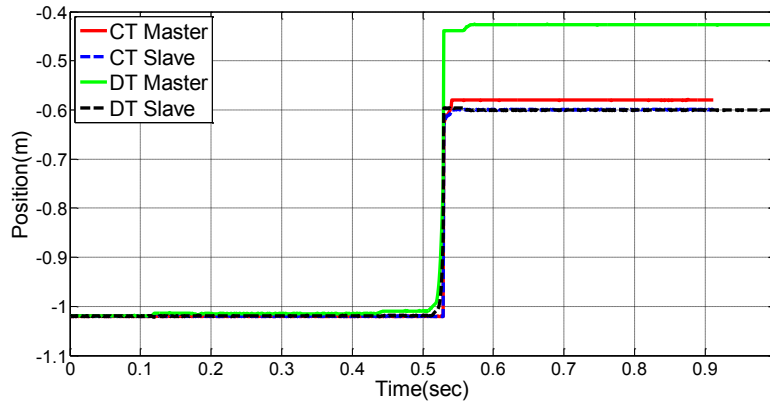


Fig. 13. Position tracking profiles for continuous-time and discrete-time teleoperation under fair comparison conditions.

10.2 Human task performance

Ten human operators (five females and five males), in their twenties, were asked to flip the switch shown in Fig. 11. The operators were engineering students with modest prior knowledge about the teleoperated three-way switch task. The human operators could only manipulate the master robot and the slave robot was the one to interact with the switch. The operator's primary goal was defined as flipping the switch in Fig. 11 from position 1 to position 2 but not to position 3 by applying appropriate forces on the master side. The operators were told that they only had 3 seconds to finish the task, which was found to be enough time.

Each operator performed five sets of trials with a short break between every other trial. In each trial, one of six different conditions (continuous-time control, discrete-time control with a 1 ms sampling period, and discrete-time control with a 10 ms sampling period; these 3 conditions were repeated with and without visual feedback to the operator from the slave side) was

presented to an operator for doing the switch-flipping task. Therefore, each user performed a total of 30 trials. The trials were presented in a randomized order to each operator. Before the experiments, each operator was given two to three practice trials until he or she felt comfortable with the operation of the master-slave system and understood the switch-flipping task.

Table 1: Success tasks rates of different control conditions

Condition \ Operator	① C-T controller with visual feedback	② C-T controller without visual feedback	③ D-T controller with T=1ms with visual feedback	④ D-T controller with T=1ms without visual feedback	⑤ D-T controller with T=10ms with visual feedback	⑥ D-T controller with T=10ms without visual feedback
Subject 1	100%	100%	40%	40%	0%	20%
Subject 2	100%	80%	40%	40%	20%	0%
Subject 3	100%	80%	20%	20%	20%	0%
Subject 4	100%	100%	20%	0%	0%	0%
Subject 5	100%	100%	40%	20%	20%	20%
Subject 6	100%	100%	40%	0%	20%	0%
Subject 7	100%	80%	40%	0%	0%	20%
Subject 8	100%	80%	20%	40%	20%	0%
Subject 9	100%	100%	40%	0%	0%	0%
Subject 10	100%	100%	20%	20%	20%	0%

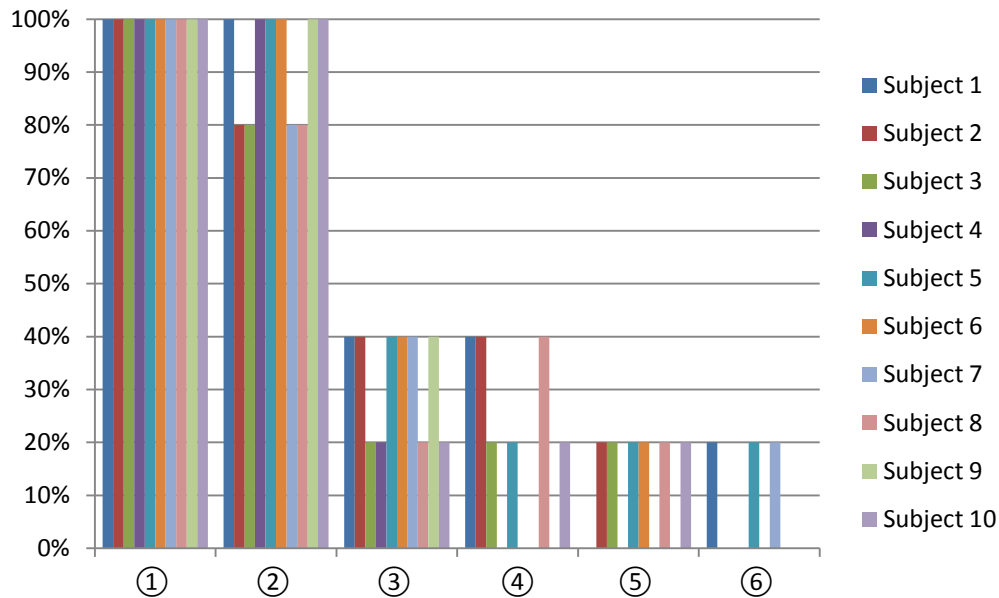


Fig. 14. Success rates of the task under different control conditions

The final results, averaged over the 30 trials for each subject, are presented numerically in Table 1 and graphically in Fig. 14. In the presence of visual feedback from the slave side for the operator, the human participants could successfully flip the switch from state 1 to state 2.

- 100% of times when using the continuous-time controlled teleoperation system①.
- 20-40% of times when using the discrete-time controlled teleoperation system with a sampling period of 1 *ms* ③.
- 0-20% of times when using the discrete-time controlled teleoperation system with a sampling period of 10 *ms* ⑤.

In the absence of visual feedback, the success rates were 80-100%, 0-40% and 0-20%, respectively (cases ②, ④, ⑥).

Therefore, with a continuous-time controlled teleoperation system the operators had the least problem performing the task. With a discrete-time controlled teleoperation system, the task success rates went down. This problem was exacerbated as the sampling period increased. The above conclusions are robust against whether or not visual feedback was provided to the human operators for this specific task.

Table 2: Right-tailed T-test results among different control conditions

Condition \ Conditions	①C-T controller with visual feedback	②C-T controller without visual feedback	③D-T controller with $T=1ms$ with visual feedback	④D-T controller with $T=1ms$ without visual feedback	⑤D-T controller with $T=10ms$ with visual feedback	⑥D-T controller with $T=10ms$ without visual feedback
①						
②	0.040563					
③	3.183E-09	8.905E-08				
④	6.310E-08	1.659E-06	0.03114			
⑤	3.234E-10	4.261E-08	0.00188	0.139436		
⑥	9.909E-11	4.257E-09	6.730E-06	0.040563	0.139436	

To ensure that the averages of the success rates reported above can be relied upon, tests of statistical significance were performed. Table 2 depicts the right-tailed t-test results. As shown in Table 2, the p-value for the t-test between ① and ② is $p = 0.040563$, which is less than the selected threshold value of statistical significance (0.05). The same can be said about cases ③ and ④. However, for cases ⑤ and ⑥, $p = 0.139436$ which is bigger than 0.05, implying that there is no statistical difference between the two cases. Overall, it can be said that providing visual feedback (①, ③) positively impacted the task success rate compared to not providing visual feedback (②, ④). Within each modality (i.e., with visual feedback and without visual feedback), ① > ③ > ⑤ and ② > ④ > ⑥ can be concluded, where “>” signifies higher success rates; note that the corresponding p-values listed in Table 2 are all less than 0.05, confirming the existence of significant differences between the corresponding pairs. Thus, irrespective of the visual feedback, the task success rate is much higher in continuous-time controlled teleoperation than in discrete-time controlled teleoperation even for a small sampling period (1 *ms*) and the performance gap widens as the sampling period increases (10 *ms*).

11. Conclusions and future work

In this article, the performance of a continuous-time controlled bilateral teleoperation system was contrasted to that of a discrete-time controlled teleoperation system in theory and experiments for a given task. The work showed that a simple, low-cost continuous-time controller can outperform discrete-time controllers in terms of task success rates. The main take-home lesson of the paper is that, in teleoperated task execution, the root causes of task failure need not necessarily be only ubiquitous non-idealities such as friction, noise, control signal saturation, un-modelled dynamics, communication channel delay, etc., but can be control sampling as well. Possible extensions of the current study include mixing the capabilities of analog and digital controllers to achieve highly transparent and stable teleoperation in haptic applications involving both soft and hard environments or both force and position control.

Acknowledgements

This research was supported by the Natural Sciences and Engineering Research Council (NSERC) of Canada, by the Canada Foundation for Innovation (CFI), and by the China Scholarship Council (CSC) under grant [2013]06120200.

References

- [1] A. Ashrafzadeh. (2007). *Analog Control vs. Digital in Power Management*. Available: www.eetasia.com/ART_8800453830_765245_NT_c4fb922a.htm
- [2] M. Hewitson, "Digital vs Analog Control," presented at the GEO ISC Meeting, 2010.
- [3] I. A. Brezovich, "Digital vs. Analogue Control Systems," presented at the the 2011 Annual Meeting of the American College of Medical Physics, 2011.
- [4] A. Malcher and P. Falkowski, "Analog Reconfigurable Circuits," *International Journal of Electronics and Telecommunications*, vol. 60 (1), pp. 15-26, 2014.
- [5] T. B. Sheridan, "Telerobotics," *Automatica*, vol. 25, pp. 487-508, 1989.
- [6] J. E. Colgate and G. G. Schenkel, "Passivity of A Class of Sampled-Data Systems: Application to Haptic Interfaces," *Journal of Robotic Systems*, vol. 14, pp. 37-47, Jan 1997.
- [7] N. Diolaiti, G. Niemeyer, F. Barbagli, and J. K. Salisbury, "Stability of Haptic Rendering: Discretization, Quantization, Time delay, and Coulomb Effects," *Ieee Transactions on Robotics*, vol. 22, pp. 256-268, Apr 2006.
- [8] D. J. Lee and M. W. Spong, "Passive Bilateral Teleoperation with Constant Time Delay," *Ieee Transactions on Robotics*, vol. 22, pp. 269-281, Apr 2006.
- [9] E. Nuno, L. Basanez, and R. Ortega, "Passivity-Based Control for Bilateral Teleoperation: A Tutorial," *Automatica*, vol. 47, pp. 485-495, Mar 2011.
- [10] J. Li, M. Tavakoli, V. Mendez, and Q. Huang, "Conservatism of Passivity Criteria for Stability Analysis of Trilateral Haptic Systems," presented at the 2013 World Haptics Conference (Whc), 2013.
- [11] R. J. Adams and B. Hannaford, "Stable Haptic Interaction with Virtual Environments," *Ieee Transactions on Robotics and Automation*, vol. 15, pp. 465-474, Jun 1999.
- [12] M. Aliaga, A. Rubio, and E. Sanchez, "Experimental Quantitative Comparison of Different Control Architectures for Master-Slave Teleoperation," *Ieee Transactions on Control Systems Technology*, vol. 12, pp. 2-11, Jan 2004.
- [13] A. Aziminejad, M. Tavakoli, R. V. Patel, and M. Moallem, "Stability and Performance in Delayed Bilateral Teleoperation: Theory and Experiments," *Control Engineering Practice*, vol. 16, pp. 1329-1343, Nov 2008.

- [14] A. Jazayeri and M. Tavakoli, "Revisiting Llewellyn's Absolute Stability Criterion for Bilateral Teleoperation Systems under Non-passive Operator or Environment," presented at the 2012 Ieee/Rsj International Conference on Intelligent Robots And Systems (Iros), 2012.
- [15] A. Jazayeri and M. Tavakoli, "Absolute Stability Analysis of Sampled-Data Scaled Bilateral Teleoperation Systems," *Control Engineering Practice*, vol. 21, pp. 1053-1064, Aug 2013.
- [16] A. Nealen, M. Muller, R. Keiser, E. Boxerman, and M. Carlson, "Physically Based Deformable Models in Computer Graphics," *Computer Graphics Forum*, vol. 25, pp. 809-836, 2006.
- [17] H. Courtecuisse, H. Jung, J. Allard, C. Duriez, D. Y. Lee, and S. Cotin, "GPU-Based Real-Time Soft Tissue Deformation with Cutting and Haptic Feedback," *Progress In Biophysics & Molecular Biology*, vol. 103, pp. 159-168, Dec 2010.
- [18] R. Mafi, S. Sirouspour, B. Mahdavihah, B. Moody, K. Elizeh, A. B. Kinsman, *et al.*, "A Parallel Computing Platform for Real-Time Haptic Interaction with Deformable Bodies," *Ieee Transactions on Haptics*, vol. 3, pp. 211-223, Jul-Sep 2010.
- [19] T. Spinner, B. Srinivasan, and R. Rengaswamy, "Data-based Automated Diagnosis and Iterative Retuning of Proportional-Integral (PI) Controllers," *Control Engineering Practice*, vol. 29, pp. 23-41, 2014.
- [20] I. Susa and Y. Takehana, "Haptic Rendering Based on Finite Element Simulation of Vibration," presented at the IEEE Haptics Symposium 2014, 2014.
- [21] A. Jazayeri and M. Tavakoli, "Stability Analysis of Sampled-Data Teleoperation Systems," *49th Ieee Conference on Decision And Control (Cdc)*, p. 6, 2010.
- [22] F. B. Llewellyn, "Some Fundamental Properties of Transmission Systems," *Proceedings of the Institute Of Radio Engineers*, vol. 40, pp. 271-283, 1952.
- [23] S. S. Haykin, *Active Network Theory*. Reading, Mass.: Addison-Wesley Pub. Co., 1970.
- [24] M. Tavakoli, Aziminejad A., "High-Fidelity Bilateral Teleoperation Systems and the Effect of Multimodal Haptics," *Ieee Transactions on Systems, Man, and Cybernetics-Part B: Cybernetics*, vol. 37, pp. 1512-1528, 2007.
- [25] K. Ogata, *Discrete-Time Control Systems, 2nd Edition*: Prentice Hall, 1995.